Measurement of the branching fraction $\mathcal{B}(\Lambda_b^0 \to \Lambda_c^+ \pi^- \pi^+ \pi^-)$ at CDF

T. Aaltonen,[21] B. Álvarez González,[9,y] S. Amerio,[40a] D. Amidei,[32] A. Anastassov,[15,w] A. Annovi,[17] J. Antos,[12] G. Apollinari,[15] J. A. Appel,[15] T. Arisawa,[54] A. Artikov,[13] J. Asaadi,[49] W. Ashmanskas,[15] B. Auerbach,[57] A. Aurisano,[49] F. Azfar,[39] P. Azzurri,[42a,42b] W. Badgett,[15] T. Bae,[25] A. Barbaro-Galtieri,[26] V. E. Barnes,[44] B. A. Barnett,[23] P. Barria,[42a,42c] P. Bartos,[12] M. Bauce,[40a,40b] F. Bedeschi,[42a] S. Behari,[23] G. Bellettini,[42a,42b] J. Bellinger,[56] D. Benjamin,[14] A. Beretvas,[15] A. Bhatti,[46] M. Binkley,[15,a] D. Bisello,[40a,40b] I. Bizjak,[28] K. R. Bland,[5] B. Blumenfeld,[23] A. Bocci,[14] A. Bodek,[45] D. Bortoletto,[44] J. Boudreau,[43] A. Boveia,[11] L. Brigliadori,[6a,6b] C. Bromberg,[33] E. Brucken,[21] J. Budagov,[13] H. S. Budd,[45] K. Burkett,[15] G. Busetto,[40a,40b] P. Bussey,[19] A. Buzatu,[31] A. Calamba,[10] C. Calancha,[29] S. Camarda,[4] M. Campanelli,[28] M. Campbell,[32] F. Canelli,[11,15] B. Carls,[22] D. Carlsmith,[56] R. Carosi,[42a] S. Carrillo,[16,m] S. Carron,[15] B. Casal,[9,k] M. Casarsa,[50a] A. Castro,[6a,6b] P. Catastini,[20] D. Cauz,[50a] V. Cavaliere,[22] M. Cavalli-Sforza,[4] A. Cerri,[26,f] L. Cerrito,[28,r] Y. C. Chen,[1] M. Chertok,[7] G. Chiarelli,[42a] G. Chlachidze,[15] F. Chlebana,[15] K. Cho,[25] D. Chokheli,[13] W. H. Chung,[56] Y. S. Chung,[45] M. A. Ciocci,[42a,42c] A. Clark,[18] C. Clarke,[55] G. Compostella,[40a,40b] M. E. Convery,[15] J. Conway,[7] M. Corbo,[15] M. Cordelli,[17] C. A. Cox,[7] D. J. Cox,[7] F. Crescioli,[42a,42b] J. Cuevas,[9,y] R. Culbertson,[15] D. Dagenhart,[15] N. d'Ascenzo,[15,v] M. Datta,[15] P. de Barbaro,[45] M. Dell'Orso,[42a,42b] L. Demortier,[46] M. Deninno,[6a] F. Devoto,[21] M. d'Errico,[40a,40b] A. Di Canto,[42a,42b] B. Di Ruzza,[15] J. R. Dittmann,[5] M. D'Onofrio,[27] S. Donati,[42a,42b] P. Dong,[15] M. Dorigo,[50a] T. Dorigo,[40a] K. Ebina,[54] A. Elagin,[49] A. Eppig,[32] R. Erbacher,[7] S. Errede,[22] N. Ershaidat,[15,cc] R. Eusebi,[49] H. C. Fang,[26] S. Farrington,[39] M. Feindt,[24] J. P. Fernandez,[29] R. Field,[16] G. Flanagan,[15,t] R. Forrest,[7] M. J. Frank,[5] M. Franklin,[20] J. C. Freeman,[15] Y. Funakoshi,[54] I. Furic,[16] M. Gallinaro,[46] J. E. Garcia,[18] A. F. Garfinkel,[44] P. Garosi,[42a,42c] H. Gerberich,[22] E. Gerchtein,[15] V. Giakoumopoulou,[3] P. Giannetti,[42a] K. Gibson,[43] C. M. Ginsburg,[15] N. Giokaris,[3] P. Giromini,[17] G. Giurgiu,[23] V. Glagolev,[13] D. Glenzinski,[15] M. Gold,[35] D. Goldin,[49] N. Goldschmidt,[16] A. Golossanov,[15] G. Gomez,[9] G. Gomez-Ceballos,[30] M. Goncharov,[30] O. González,[29] I. Gorelov,[35] A. T. Goshaw,[14] K. Goulianos,[46] S. Grinstein,[4] C. Grosso-Pilcher,[11] R. C. Group,[53,15] J. Guimaraes da Costa,[20] Z. Gunay-Unalan,[33] C. Haber,[26] S. R. Hahn,[15] E. Halkiadakis,[48] A. Hamaguchi,[38] J. Y. Han,[45] F. Happacher,[17] K. Hara,[51] D. Hare,[48] M. Hare,[52] R. F. Harr,[55] K. Hatakeyama,[5] C. Hays,[39] M. Heck,[24] J. Heinrich,[41] M. Herndon,[56] S. Hewamanage,[5] A. Hocker,[15] W. Hopkins,[15,g] D. Horn,[24] S. Hou,[1] R. E. Hughes,[36] M. Hurwitz,[11] U. Husemann,[57] N. Hussain,[31] M. Hussein,[33] J. Huston,[33] G. Introzzi,[42a] M. Iori,[47a,47b] A. Ivanov,[7,p] E. James,[15] D. Jang,[10] B. Jayatilaka,[14] E. J. Jeon,[25] S. Jindariani,[15] W. Johnson,[7] M. Jones,[44] K. K. Joo,[25] S. Y. Jun,[10] T. R. Junk,[15] T. Kamon,[49] P. E. Karchin,[55] A. Kasmi,[5] Y. Kato,[38,o] W. Ketchum,[11] J. Keung,[41] V. Khotilovich,[49] B. Kilminster,[15] D. H. Kim,[25] H. S. Kim,[25] J. E. Kim,[25] M. J. Kim,[17] S. B. Kim,[25] S. H. Kim,[51] Y. K. Kim,[11] Y. J. Kim,[25] N. Kimura,[54] M. Kirby,[15] K. Knoepfel,[15] K. Kondo,[54,a] D. J. Kong,[25] J. Konigsberg,[16] A. V. Kotwal,[14] M. Kreps,[24] J. Kroll,[41] D. Krop,[11] M. Kruse,[14] V. Krutelyov,[49,d] T. Kuhr,[24] M. Kurata,[51] S. Kwang,[11] A. T. Laasanen,[44] S. Lami,[42a] S. Lammel,[15] M. Lancaster,[28] R. L. Lander,[7] K. Lannon,[36,x] A. Lath,[48] G. Latino,[42a,42b] T. LeCompte,[2] E. Lee,[49] H. S. Lee,[11] J. S. Lee,[25] S. W. Lee,[49,aa] S. Leo,[42a,42b] S. Leone,[42a] J. D. Lewis,[15] A. Limosani,[14,s] C.-J. Lin,[26] J. Linacre,[39] M. Lindgren,[15] E. Lipeles,[41] A. Lister,[18] D. O. Litvintsev,[15] C. Liu,[43] H. Liu,[53] Q. Liu,[44] T. Liu,[15] S. Lockwitz,[57] A. Loginov,[57] D. Lucchesi,[40a,40b] J. Lueck,[24] P. Lujan,[26] P. Lukens,[15] G. Lungu,[46] J. Lys,[26] R. Lysak,[12] R. Madrak,[15] K. Maeshima,[15] P. Maestro,[42a,42c] S. Malik,[46] G. Manca,[27,b] A. Manousakis-Katsikakis,[3] F. Margaroli,[47a] C. Marino,[24] M. Martínez,[4] K. Matera,[22] M. E. Mattson,[55] A. Mazzacane,[15] P. Mazzanti,[6a] K. S. McFarland,[45] P. McIntyre,[49] R. McNulty,[27,j] A. Mehta,[27] P. Mehtala,[21] C. Mesropian,[46] T. Miao,[15] D. Mietlicki,[32] A. Mitra,[1] H. Miyake,[51] S. Moed,[15] N. Moggi,[6a] M. N. Mondragon,[15,m] C. S. Moon,[25] R. Moore,[15] M. J. Morello,[42a,42d] J. Morlock,[24] P. Movilla Fernandez,[15] A. Mukherjee,[15] Th. Muller,[24] P. Murat,[15] M. Mussini,[6a,6b] J. Nachtman,[15,n] Y. Nagai,[51] J. Naganoma,[54] I. Nakano,[37] A. Napier,[52] J. Nett,[49] C. Neu,[53] M. S. Neubauer,[22] J. Nielsen,[26,e] L. Nodulman,[2] S. Y. Noh,[25] O. Norniella,[22] L. Oakes,[39] S. H. Oh,[14] Y. D. Oh,[25] I. Oksuzian,[53] T. Okusawa,[38] R. Orava,[21] L. Ortolan,[4] S. Pagan Griso,[40a,40b] C. Pagliarone,[50a] E. Palencia,[9,f] V. Papadimitriou,[15] A. A. Paramonov,[2] J. Patrick,[15] G. Pauletta,[50a,50b] M. Paulini,[10] C. Paus,[30] D. E. Pellett,[7] A. Penzo,[50a] T. J. Phillips,[14] G. Piacentino,[42a] E. Pianori,[41] J. Pilot,[36] K. Pitts,[22] C. Plager,[8] L. Pondrom,[56] S. Poprocki,[15,g] K. Potamianos,[44] O. Poukhov,[13,a] F. Prokoshin,[13,bb] A. Pranko,[26] F. Ptohos,[17,h] G. Punzi,[42a,42b] A. Rahaman,[43] V. Ramakrishnan,[56] N. Ranjan,[44] I. Redondo,[29] P. Renton,[39] M. Rescigno,[47a] T. Riddick,[28] F. Rimondi,[6a,6b] L. Ristori,[42a,15] A. Robson,[19] T. Rodrigo,[9] T. Rodriguez,[41] E. Rogers,[22] S. Rolli,[52,i] R. Roser,[15] F. Ruffini,[42a,42c] A. Ruiz,[9] J. Russ,[10] V. Rusu,[15] A. Safonov,[49] W. K. Sakumoto,[45] Y. Sakurai,[54] L. Santi,[50a,50b] K. Sato,[51] V. Saveliev,[15,v] A. Savoy-Navarro,[15,z] P. Schlabach,[15] A. Schmidt,[24] E. E. Schmidt,[15] M. P. Schmidt,[57,a] T. Schwarz,[15] L. Scodellaro,[9] A. Scribano,[42a,42c] F. Scuri,[42a] S. Seidel,[35] Y. Seiya,[38] A. Semenov,[13] F. Sforza,[42a,42c] S. Z. Shalhout,[7] T. Shears,[27] P. F. Shepard,[43] M. Shimojima,[51,u] M. Shochet,[11] I. Shreyber-Tecker,[34]

A. Simonenko,[13] P. Sinervo,[31] A. Sissakian,[13,a] K. Sliwa,[52] J. R. Smith,[7] F. D. Snider,[15] A. Soha,[15] V. Sorin,[4] P. Squillacioti,[42a,42c] M. Stancari,[15] R. St. Denis,[19] B. Stelzer,[31] O. Stelzer-Chilton,[31] D. Stentz,[15,w] J. Strologas,[35] G. L. Strycker,[32] Y. Sudo,[51] A. Sukhanov,[15] I. Suslov,[13] K. Takemasa,[51] Y. Takeuchi,[51] J. Tang,[11] M. Tecchio,[32] P. K. Teng,[1] J. Thom,[15,g] J. Thome,[10] G. A. Thompson,[22] E. Thomson,[41] D. Toback,[49] S. Tokar,[12] K. Tollefson,[33] T. Tomura,[51] D. Tonelli,[15] S. Torre,[17] D. Torretta,[15] P. Totaro,[40a] M. Trovato,[42a,42d] Y. Tu,[41] F. Ukegawa,[51] S. Uozumi,[25] A. Varganov,[32] E. Vataga,[42a,42b] F. Vázquez,[16,m] G. Velev,[15] C. Vellidis,[15] M. Vidal,[44] I. Vila,[9] R. Vilar,[9] J. Vizán,[9] M. Vogel,[35] G. Volpi,[17] P. Wagner,[41] R. L. Wagner,[15] T. Wakisaka,[38] R. Wallny,[8] S. M. Wang,[1] A. Warburton,[31] D. Waters,[28] W. C. Wester III,[15] D. Whiteson,[41,c] A. B. Wicklund,[2] E. Wicklund,[15] S. Wilbur,[11] F. Wick,[24] H. H. Williams,[41] J. S. Wilson,[36] P. Wilson,[15] B. L. Winer,[36] P. Wittich,[15,g] S. Wolbers,[15] H. Wolfe,[36] T. Wright,[32] X. Wu,[18] Z. Wu,[5] K. Yamamoto,[38] D. Yamato,[38] T. Yang,[15] U. K. Yang,[11,q] Y. C. Yang,[25] W.-M. Yao,[26] G. P. Yeh,[15] K. Yi,[15,n] J. Yoh,[15] K. Yorita,[54] T. Yoshida,[38,l] G. B. Yu,[14] I. Yu,[25] S. S. Yu,[15] J. C. Yun,[15] A. Zanetti,[50a] Y. Zeng,[14] and S. Zucchelli[6a,6b]

(CDF Collaboration)

[1]*Institute of Physics, Academia Sinica, Taipei, Taiwan 11529, Republic of China*
[2]*Argonne National Laboratory, Argonne, Illinois 60439, USA*
[3]*University of Athens, 157 71 Athens, Greece*
[4]*Institut de Fisica d'Altes Energies, ICREA, Universitat Autonoma de Barcelona, E-08193, Bellaterra (Barcelona), Spain*
[5]*Baylor University, Waco, Texas 76798, USA*
[6a]*Istituto Nazionale di Fisica Nucleare Bologna, I-40127 Bologna, Italy*
[6b]*University of Bologna, I-40127 Bologna, Italy*
[7]*University of California, Davis, Davis, California 95616, USA*
[8]*University of California, Los Angeles, Los Angeles, California 90024, USA*
[9]*Instituto de Fisica de Cantabria, CSIC-University of Cantabria, 39005 Santander, Spain*
[10]*Carnegie Mellon University, Pittsburgh, Pennsylvania 15213, USA*
[11]*Enrico Fermi Institute, University of Chicago, Chicago, Illinois 60637, USA*
[12]*Comenius University, 842 48 Bratislava, Slovakia; Institute of Experimental Physics, 040 01 Kosice, Slovakia*
[13]*Joint Institute for Nuclear Research, RU-141980 Dubna, Russia*
[14]*Duke University, Durham, North Carolina 27708, USA*
[15]*Fermi National Accelerator Laboratory, Batavia, Illinois 60510, USA*
[16]*University of Florida, Gainesville, Florida 32611, USA*
[17]*Laboratori Nazionali di Frascati, Istituto Nazionale di Fisica Nucleare, I-00044 Frascati, Italy*
[18]*University of Geneva, CH-1211 Geneva 4, Switzerland*
[19]*Glasgow University, Glasgow G12 8QQ, United Kingdom*
[20]*Harvard University, Cambridge, Massachusetts 02138, USA*
[21]*Division of High Energy Physics, Department of Physics, University of Helsinki and Helsinki Institute of Physics, FIN-00014, Helsinki, Finland*
[22]*University of Illinois, Urbana, Illinois 61801, USA*
[23]*The Johns Hopkins University, Baltimore, Maryland 21218, USA*
[24]*Institut für Experimentelle Kernphysik, Karlsruhe Institute of Technology, D-76131 Karlsruhe, Germany*
[25]*Center for High Energy Physics, Kyungpook National University, Daegu 702-701, Korea; Seoul National University, Seoul 151-742, Korea; Sungkyunkwan University, Suwon 440-746, Korea; Korea Institute of Science and Technology Information, Daejeon 305-806, Korea; Chonnam National University, Gwangju 500-757, Korea; Chonbuk National University, Jeonju 561-756, Korea*
[26]*Ernest Orlando Lawrence Berkeley National Laboratory, Berkeley, California 94720, USA*
[27]*University of Liverpool, Liverpool L69 7ZE, United Kingdom*
[28]*University College London, London WC1E 6BT, United Kingdom*
[29]*Centro de Investigaciones Energeticas Medioambientales y Tecnologicas, E-28040 Madrid, Spain*
[30]*Massachusetts Institute of Technology, Cambridge, Massachusetts 02139, USA*
[31]*Institute of Particle Physics, McGill University, Montréal, Québec, Canada H3A 2T8; Simon Fraser University, Burnaby, British Columbia, Canada V5A 1S6; University of Toronto, Toronto, Ontario, Canada M5S 1A7; and TRIUMF, Vancouver, British Columbia, Canada V6T 2A3*
[32]*University of Michigan, Ann Arbor, Michigan 48109, USA*
[33]*Michigan State University, East Lansing, Michigan 48824, USA*
[34]*Institution for Theoretical and Experimental Physics, ITEP, Moscow 117259, Russia*

[35]*University of New Mexico, Albuquerque, New Mexico 87131, USA*
[36]*The Ohio State University, Columbus, Ohio 43210, USA*
[37]*Okayama University, Okayama 700-8530, Japan*
[38]*Osaka City University, Osaka 588, Japan*
[39]*University of Oxford, Oxford OX1 3RH, United Kingdom*
[40a]*Istituto Nazionale di Fisica Nucleare, Sezione di Padova-Trento, I-35131 Padova, Italy*
[40b]*University of Padova, I-35131 Padova, Italy*
[41]*University of Pennsylvania, Philadelphia, Pennsylvania 19104, USA*
[42a]*Istituto Nazionale di Fisica Nucleare Pisa, I-56127 Pisa, Italy*
[42b]*University of Pisa, I-56127 Pisa, Italy*
[42c]*University of Siena, I-56127 Pisa, Italy*
[42d]*Scuola Normale Superiore, I-56127 Pisa, Italy*
[43]*University of Pittsburgh, Pittsburgh, Pennsylvania 15260, USA*
[44]*Purdue University, West Lafayette, Indiana 47907, USA*
[45]*University of Rochester, Rochester, New York 14627, USA*
[46]*The Rockefeller University, New York, New York 10065, USA*
[47a]*Istituto Nazionale di Fisica Nucleare, Sezione di Roma 1, I-00185 Roma, Italy*
[47b]*Sapienza Università di Roma, I-00185 Roma, Italy*
[48]*Rutgers University, Piscataway, New Jersey 08855, USA*
[49]*Texas A&M University, College Station, Texas 77843, USA*
[50a]*Istituto Nazionale di Fisica Nucleare Trieste/Udine, I-34100 Trieste, Italy*
[50b]*University of Udine, I-33100 Udine, Italy*
[51]*University of Tsukuba, Tsukuba, Ibaraki 305, Japan*
[52]*Tufts University, Medford, Massachusetts 02155, USA*
[53]*University of Virginia, Charlottesville, Virginia 22906, USA*
[54]*Waseda University, Tokyo 169, Japan*
[55]*Wayne State University, Detroit, Michigan 48201, USA*
[56]*University of Wisconsin, Madison, Wisconsin 53706, USA*
[57]*Yale University, New Haven, Connecticut 06520, USA*
(Received 14 December 2011; published 13 February 2012)

[a]Deceased
[b]Visitor from Istituto Nazionale di Fisica Nucleare, Sezione di Cagliari, 09042 Monserrato (Cagliari), Italy
[c]Visitor from University of California, Irvine, Irvine, CA 92697, USA
[d]Visitor from University of California, Santa Barbara, Santa Barbara, CA 93106, USA
[e]Visitor from University of California, Santa Cruz, Santa Cruz, CA 95064, USA
[f]Visitor from CERN, CH-1211 Geneva, Switzerland
[g]Visitor from Cornell University, Ithaca, NY 14853, USA
[h]Visitor from University of Cyprus, Nicosia CY-1678, Cyprus
[i]Visitor from Office of Science, U.S. Department of Energy, Washington, DC 20585, USA
[j]Visitor from University College Dublin, Dublin 4, Ireland
[k]Visitor from ETH, 8092 Zurich, Switzerland
[l]Visitor from University of Fukui, Fukui City, Fukui Prefecture, Japan 910-0017
[m]Visitor from Universidad Iberoamericana, Mexico D.F., Mexico
[n]Visitor from University of Iowa, Iowa City, IA 52242, USA
[o]Visitor from Kinki University, Higashi-Osaka City, Japan 577-8502
[p]Visitor from Kansas State University, Manhattan, KS 66506, USA
[q]Visitor from University of Manchester, Manchester M13 9PL, United Kingdom
[r]Visitor from Queen Mary, University of London, London, E1 4NS, United Kingdom
[s]Visitor from University of Melbourne, Victoria 3010, Australia
[t]Visitor from Muons, Inc., Batavia, IL 60510, USA
[u]Visitor from Nagasaki Institute of Applied Science, Nagasaki, Japan
[v]Visitor from National Research Nuclear University, Moscow, Russia
[w]Visitor from Northwestern University, Evanston, IL 60208, USA
[x]Visitor from University of Notre Dame, Notre Dame, IN 46556, USA
[y]Visitor from Universidad de Oviedo, E-33007 Oviedo, Spain
[z]Visitor from CNRS-IN2P3, Paris, F-75252 France
[aa]Visitor from Texas Tech University, Lubbock, TX 79609, USA
[bb]Visitor from Universidad Tecnica Federico Santa Maria, 110v Valparaiso, Chile
[cc]Visitor from Yarmouk University, Irbid 211-63, Jordan

We report an analysis of the $\Lambda_b^0 \to \Lambda_c^+ \pi^- \pi^+ \pi^-$ decay in a data sample collected by the CDF II detector at the Fermilab Tevatron corresponding to 2.4 fb^{-1} of integrated luminosity. We reconstruct the currently largest samples of the decay modes $\Lambda_b^0 \to \Lambda_c(2595)^+ \pi^-$ (with $\Lambda_c(2595)^+ \to \Lambda_c^+ \pi^+ \pi^-$), $\Lambda_b^0 \to \Lambda_c(2625)^+ \pi^-$ (with $\Lambda_c(2625)^+ \to \Lambda_c^+ \pi^+ \pi^-$), $\Lambda_b^0 \to \Sigma_c(2455)^{++} \pi^- \pi^-$ (with $\Sigma_c(2455)^{++} \to \Lambda_c^+ \pi^+$), and $\Lambda_b^0 \to \Sigma_c(2455)^0 \pi^+ \pi^-$ (with $\Sigma_c(2455)^0 \to \Lambda_c^+ \pi^-$) and measure the branching fractions relative to the $\Lambda_b^0 \to \Lambda_c^+ \pi^-$ branching fraction. We measure the ratio $\mathcal{B}(\Lambda_b^0 \to \Lambda_c^+ \pi^- \pi^+ \pi^-)/\mathcal{B}(\Lambda_b^0 \to \Lambda_c^+ \pi^-) = 3.04 \pm 0.33(\text{stat})^{+0.70}_{-0.55}(\text{syst})$ which is used to derive $\mathcal{B}(\Lambda_b^0 \to \Lambda_c^+ \pi^- \pi^+ \pi^-) = (26.8^{+11.9}_{-11.2}) \times 10^{-3}$.

DOI: 10.1103/PhysRevD.85.032003 PACS numbers: 14.20.Mr, 14.20.Lq

I. INTRODUCTION

Because of the high b-quark mass, weak decays of baryons containing a b quark are a good testing ground of some approximations in quantum chromodynamics calculations, such as heavy-quark effective theory [1]. Alternatively, when one uses such calculations, the Λ_b^0 may provide a determination of the Cabibbo-Kobayashi-Maskawa couplings with systematic uncertainties different from the determinations from the decays of B mesons [2]. While the B mesons are well studied, less is known about the Λ_b^0 baryon. Only nine decay modes of the Λ_b^0 have been observed so far, with the sum of their measured branching fractions of the order of only 0.1 and with large uncertainties on the measurements [3]. While theoretical predictions are available for the $\Lambda_b^0 \to \Lambda_c^+ \pi^-$ branching fraction [4], no prediction is currently available for the $\Lambda_b^0 \to \Lambda_c^+ \pi^- \pi^+ \pi^-$ decay mode. The LHCb Collaboration recently reported the measurement of the ratio of branching fractions $\mathcal{B}(\Lambda_b^0 \to \Lambda_c^+ \pi^- \pi^+ \pi^-)/\mathcal{B}(\Lambda_b^0 \to \Lambda_c^+ \pi^-) = 1.43 \pm 0.16(\text{stat}) \pm 0.13(\text{syst})$ [5].

This paper reports a study of the $\Lambda_b^0 \to \Lambda_c^+ \pi^- \pi^+ \pi^-$ decay mode and is especially distinguished by the high yields and high precision measurement of the $\Lambda_b^0 \to \Lambda_c^+ \pi^- \pi^+ \pi^-$ resonant contributions, the following decay modes:

$$\Lambda_b^0 \to \Lambda_c(2595)^+ \pi^-, \qquad \Lambda_b^0 \to \Lambda_c(2625)^+ \pi^-,$$
$$\Lambda_b^0 \to \Sigma_c(2455)^{++} \pi^- \pi^-, \qquad \Lambda_b^0 \to \Sigma_c(2455)^0 \pi^+ \pi^-.$$

We measure the branching fraction of each resonant decay mode relative to the $\Lambda_b^0 \to \Lambda_c^+ \pi^-$ decay mode, and the ratio of branching fractions $\mathcal{B}(\Lambda_b^0 \to \Lambda_c^+ \pi^- \pi^+ \pi^-)/\mathcal{B}(\Lambda_b^0 \to \Lambda_c^+ \pi^-)$. The measurement is performed using a sample of $p\bar{p}$ collisions corresponding to 2.4 fb^{-1} integrated luminosity collected by CDF II between February 2002 and May 2007. We reconstruct Λ_b^0 decays from particles whose trajectory projections in the plane transverse to the beam line do not intersect the beam line (displaced tracks). The signal yields of interest are extracted by fitting mass differences to minimize the effect of systematic uncertainties. As a cross-check, we repeat the analysis on the reference decay modes $B^0 \to D^- \pi^+ \pi^- \pi^+$ and $B^0 \to D^- \pi^+$.

The structure of the paper is as follows. Section II describes the detector systems relevant to this analysis. Event selection and $\Lambda_b^0 \to \Lambda_c^+ \pi^- \pi^+ \pi^-$ and $\Lambda_b^0 \to \Lambda_c^+ \pi^-$ candidate reconstruction are described in Sec. III. In Sec. IV we present the signal yields. In Sec. V we describe the evaluation of the detector acceptance and the relative branching fraction measurements, while in Sec. VI the systematic uncertainties are discussed. Final results are reported in Sec. VII, and we conclude in Sec. VIII.

II. THE CDF II DETECTOR AND TRIGGER

The CDF II detector is a multipurpose magnetic spectrometer surrounded by calorimeters and muon detectors. The components relevant to this analysis are briefly described here. A more detailed description can be found elsewhere [6]. A silicon microstrip detector (SVX and ISL) [7] and a cylindrical drift chamber (COT) [8] immersed in a 1.4 T solenoidal magnetic field allow the reconstruction of charged particle trajectories in the pseudorapidity [9] range $|\eta| < 1.0$ [10]. The SVX detector consists of microstrip sensors arranged in six cylindrical shells around the beam line with radii of between 1.5 and 10.6 cm, and with a total z coverage of 90 cm. The first SVX layer, also referred to as the L00 detector, is made of single-sided sensors mounted on the beryllium beam pipe. The remaining five SVX layers are made of double-sided sensors and divided into three contiguous five-layer sections along the beam direction z. The two additional silicon layers of the ISL help to link tracks in the COT to hits in the SVX. The COT has 96 measurement layers between 40 and 137 cm in radius, organized into alternating axial and $\pm 2°$ stereo superlayers. The charged particle transverse momentum resolution is $\sigma_{p_T}/p_T \simeq 0.07\% p_T$ (GeV/c), and the resolution on the transverse distance of closest approach of the particle trajectory to the beam line (impact parameter, d_0) is ≈ 40 μm, including a ≈ 30 μm contribution from the beam line.

Candidate events for this analysis are selected by a three-level online event selection system (trigger). At level 1, charged particles are reconstructed in the COT axial superlayers by a hardware processor, the "extremely fast tracker" (XFT) [11]. Two charged particles are required with transverse momenta $p_T \geq 2$ GeV/c. At level 2, the Silicon Vertex Trigger (SVT) [12] associates SVX $r - \phi$

position measurements with XFT tracks. This provides a precise measurement of the track impact parameter d_0. We select b-hadron candidates by requiring two SVT tracks with $120\ \mu\text{m} \leq d_0 \leq 1000\ \mu\text{m}$. To reduce background from light-quark jet pairs, the two trigger tracks are required to have an opening angle in the transverse plane of $2^\circ \leq \Delta\phi \leq 90^\circ$. The tracks must also satisfy the requirement $L_T > 200\ \mu$m, where L_T is defined as the distance in the transverse plane from the beam line to the two-track intersection point, projected onto the two-track momentum vector. The level 1 and level 2 trigger requirements are then confirmed at trigger level 3, where the event is fully reconstructed.

III. EVENT RECONSTRUCTION

The search for $\Lambda_b^0 \to \Lambda_c^+ \pi^- \pi^+ \pi^-$ and $\Lambda_b^0 \to \Lambda_c^+ \pi^-$ candidates begins with the reconstruction of the Λ_c^+ using the three-body decay $\Lambda_c^+ \to pK^-\pi^+$ [13]. Three tracks, assumed to be a kaon, a proton, and a pion, with a total charge of $+1$, are fit to a common vertex. No particle identification is used in this analysis. All particle hypotheses consistent with the candidate decay chain are considered. Additional selection criteria (cuts) are applied on fit probability ($P(\chi^2(\Lambda_c^+)) > 10^{-5}$), transverse momentum ($p_T(\Lambda_c^+) > 4.0$ GeV/c), and transverse decay length relative to the beam line ($L_T(\Lambda_c^+) > 200\ \mu$m). We also require $p_T(p) > p_T(\pi^+)$, to suppress random-track combinatorial background. The reconstructed Λ_c^+ mass ($m(\Lambda_c^+)$) distribution is comparable to the one reported in Ref. [14]. The reconstructed Λ_c^+ mass is required to be close to the known Λ_c^+ mass (2.240–2.330 GeV/c^2) [3]. Since mass differences are used to search for the resonances, no mass constraint is applied in the Λ_c^+ reconstruction. The $\Lambda_b^0 \to \Lambda_c^+ \pi^- \pi^+ \pi^-$ ($\Lambda_b^0 \to \Lambda_c^+ \pi^-$) candidate is reconstructed by performing a fit to a common vertex of the reconstructed Λ_c^+ and three (one) additional tracks, assumed to be pions, with $p_T > 0.4$ GeV/c, and a total charge of -1. For all the possible track pairs out of the six (four) tracks that form the Λ_b^0 candidate, we require the difference between the z coordinate of the points of closest approach of the two tracks to the beam to be less than 5 cm. Additional cuts on the Λ_b^0 candidate fit probability ($P(\chi^2(\Lambda_b^0)) > 10^{-4}$), transverse momentum ($p_T(\Lambda_b^0) > 6.0$ GeV/c), transverse decay length relative to the beam line ($L_T(\Lambda_b^0) > 200\ \mu$m), and Λ_c^+ transverse decay length relative to the beam line ($L_T(\Lambda_c^+) > 200\ \mu$m) and to the Λ_b^0 vertex ($L_T(\Lambda_c^+ \text{from} \Lambda_b^0) > -200\ \mu$m) are applied. We also require that the transverse momentum of the pion produced in the Λ_c^+ decay is larger than the transverse momentum of the same-charge pion produced in the Λ_b^0 decay, which considerably reduces the combinatorial background due to the larger boost of the pion produced in the Λ_c^+ decay. To improve the purity of the $\Lambda_b^0 \to \Lambda_c^+ \pi^- \pi^+ \pi^-$ signal, we optimize the analysis cuts to maximize the signal significance $\mathcal{S}/\sqrt{\mathcal{S}+\mathcal{B}}$. The number of $\Lambda_b^0 \to \Lambda_c^+ \pi^- \pi^+ \pi^-$ candidates $\mathcal{S}$ and the number of background events $\mathcal{B}$ are estimated in data by performing a fit of the $m(\Lambda_b^0)$ distribution. This procedure determines the final selection criteria: $p_T(\Lambda_b^0) > 9.0$ GeV/c, $L_T(\Lambda_b^0)/\sigma_{L_T(\Lambda_b^0)} > 16$, $d_0(\Lambda_b^0) < 70\ \mu$m, and $\Delta R(\pi^-\pi^+\pi^-) < 1.2$, where $d_0(\Lambda_b^0)$ is the impact parameter of the reconstructed Λ_b^0 candidate relative to the beam line and $\Delta R(\pi^-\pi^+\pi^-)$ is the maximum $\sqrt{\Delta\eta^2 + \Delta\phi^2}$ distance between the two pions in each of the three possible pairs of pions. We verified that, by splitting the data sample in two independent samples, the optimization procedure yields the same final selection criteria when applied separately to the two samples, and that the $\Lambda_b^0 \to \Lambda_c^+ \pi^- \pi^+ \pi^-$ yield is evenly

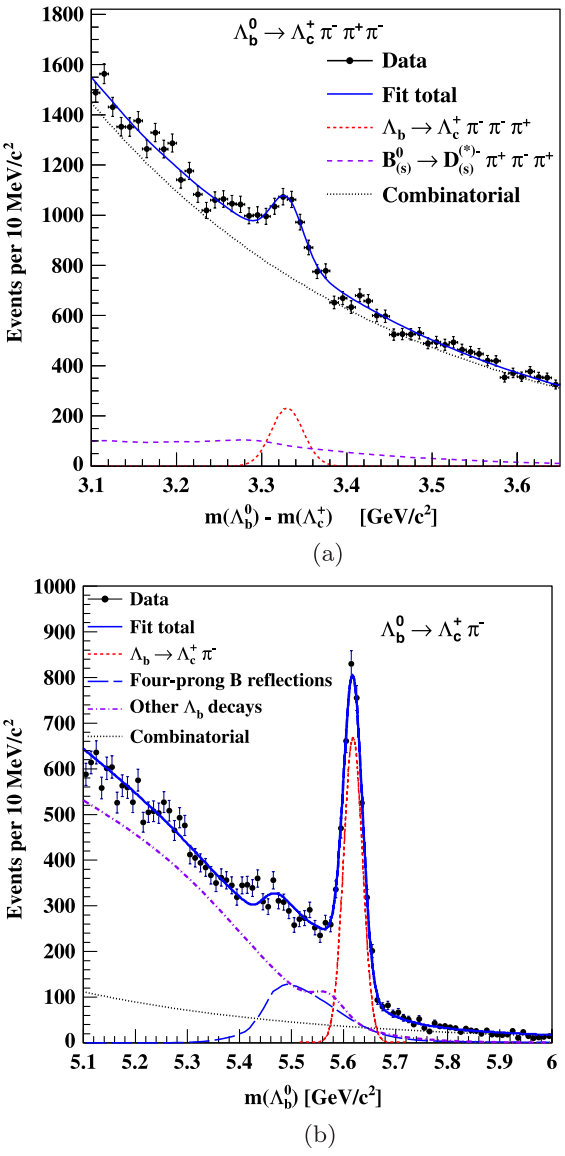

FIG. 1 (color online). The reconstructed invariant mass spectra after applying all the selection criteria: (a) the mass difference $m(\Lambda_b^0) - m(\Lambda_c^+)$ distribution of the $\Lambda_b^0 \to \Lambda_c^+ \pi^- \pi^+ \pi^-$ candidates; (b) the $m(\Lambda_b^0)$ distribution of the $\Lambda_b^0 \to \Lambda_c^+ \pi^-$ candidates.

distributed. This ensures that our optimization procedure does not introduce a bias on the branching fraction measurement. To reduce possible systematic effects in the estimate of the reconstruction efficiency due to Monte Carlo simulation model inaccuracy, the same selection cuts optimized for $\Lambda_b^0 \to \Lambda_c^+ \pi^- \pi^+ \pi^-$ are also applied to the selection of the $\Lambda_b^0 \to \Lambda_c^+ \pi^-$ signal, except for the $\Delta R(\pi^- \pi^+ \pi^-)$ cut.

IV. DETERMINATION OF THE SIGNAL YIELDS

Figure 1(a) shows the distribution of the difference between the reconstructed Λ_b^0 and Λ_c^+ masses, $m(\Lambda_b^0) - m(\Lambda_c^+)$, of the selected $\Lambda_b^0 \to \Lambda_c^+ \pi^- \pi^+ \pi^-$ candidates with the fit projection overlaid. A significant signal of $\Lambda_b^0 \to \Lambda_c^+ \pi^- \pi^+ \pi^-$ is visible centered approximately at 3.330 GeV/c^2. Backgrounds include misreconstructed multibody b-hadron decays (physics background) and

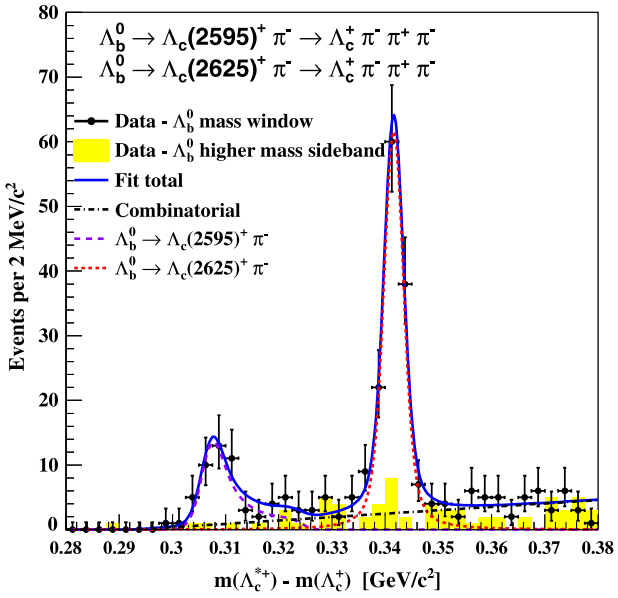

(a)

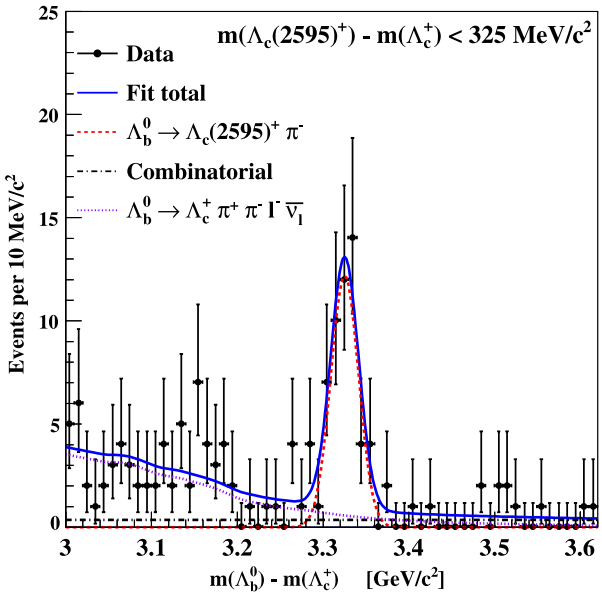

(b)

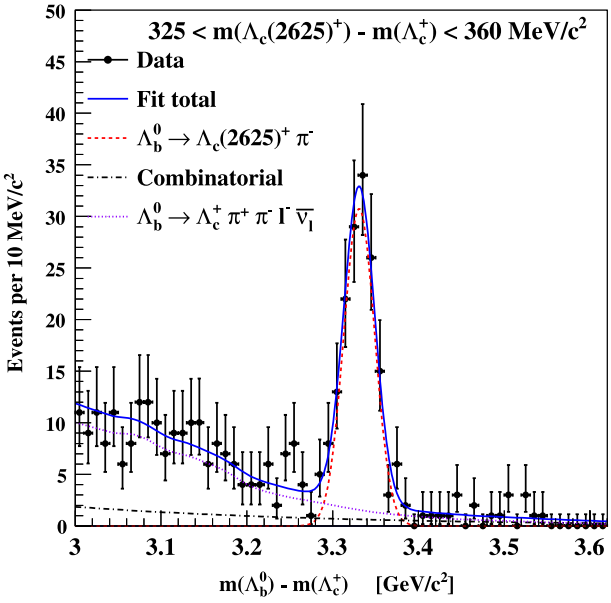

(c)

FIG. 2 (color online). The $\Lambda_b^0 \to \Lambda_c(2595)^+ \pi^-$ and $\Lambda_b^0 \to \Lambda_c(2625)^+ \pi^-$ signals: (a) $m(\Lambda_c^{*+}) - m(\Lambda_c^+)$ distribution for candidates in a $\pm 3\sigma$ range ($\pm$ 57 MeV/c^2) around the Λ_b^0 mass; (b) $m(\Lambda_b^0) - m(\Lambda_c^+)$ distribution restricted to candidates in the region $m(\Lambda_c^{*+}) - m(\Lambda_c^+) < 0.325$ GeV/c^2; (c) $m(\Lambda_b^0) - m(\Lambda_c^+)$ distribution restricted to candidates in the region $0.325 < m(\Lambda_c^{*+}) - m(\Lambda_c^+) < 0.360$ GeV/c^2.

random combinations of charged particles that accidentally meet the selection requirements (combinatorial background). We use an unbinned extended maximum-likelihood fit to estimate the $\Lambda_b^0 \to \Lambda_c^+ \pi^- \pi^+ \pi^-$ signal yield. The signal peak is modeled with a Gaussian, with mean and width left floating in the fit. The combinatorial background is modeled with an exponential function of $m(\Lambda_b^0) - m(\Lambda_c^+)$ with floating slope and normalization. The distribution of the main physics backgrounds, due to the $B_{(s)}^0 \to D_{(s)}^{(*)-} \pi^+ \pi^- \pi^+$ decay modes, are derived from simulation and included in the fit with fixed shape and floating normalization. The $\Lambda_b^0 \to \Lambda_c^+ \pi^- \pi^+ \pi^-$ yield estimated by the fit of the data is 1087 ± 101 candidates, the world's largest sample currently available of this decay mode. Figure 1(b) shows the Λ_b^0 mass distribution of the selected $\Lambda_b^0 \to \Lambda_c^+ \pi^-$ candidates. The Λ_b^0 mass distribution is described by several components: the $\Lambda_b^0 \to \Lambda_c^+ \pi^-$ Gaussian signal, a combinatorial background, reconstructed B mesons that pass the $\Lambda_c^+ \pi^-$ selection criteria, partially reconstructed Λ_b^0 decays (e.g. $\Lambda_b^0 \to \Lambda_c^+ l^- \bar{\nu}_l$), and fully reconstructed Λ_b^0 decays other than $\Lambda_c^+ \pi^-$ (e.g. $\Lambda_b^0 \to \Lambda_c^+ K^-$). Also in this case the distributions of physics backgrounds are derived from simulation and included in the fit with fixed shapes and floating normalization, as detailed in Ref. [15]. The $\Lambda_b^0 \to \Lambda_c^+ \pi^-$ yield estimated by the fit of the data is 3052 ± 78 candidates.

In the reconstructed $\Lambda_b^0 \to \Lambda_c^+ \pi^- \pi^+ \pi^-$ sample we searched for the resonant decay modes: $\Lambda_b^0 \to \Lambda_c(2595)^+ \pi^-$, $\Lambda_b^0 \to \Lambda_c(2625)^+ \pi^-$, $\Lambda_b^0 \to \Sigma_c(2455)^{++} \pi^- \pi^-$, and $\Lambda_b^0 \to \Sigma_c(2455)^0 \pi^+ \pi^-$. The available energy transferred to the decay products in the decays of the charmed baryons ($\Lambda_c(2595)^+$, $\Lambda_c(2625)^+$, $\Sigma_c(2455)^{++}$, and $\Sigma_c(2455)^0$) into Λ_c^+ is small. Therefore the differences of the reconstructed masses $m(\Lambda_c^{*+}) - m(\Lambda_c^+)$, $m(\Sigma_c(2455)^{++}) - m(\Lambda_c^+)$, and $m(\Sigma_c(2455)^0) - m(\Lambda_c^+)$ are determined with better resolution than the masses of the charmed baryons, since the mass resolution of the Λ_c^+ signal and most of the mass systematic uncertainties cancel in the difference. Figure 2(a) shows the $m(\Lambda_c^{*+}) - m(\Lambda_c^+)$ distribution, for $\Lambda_b^0 \to \Lambda_c^+ \pi^- \pi^+ \pi^-$ candidates with mass in a $\pm 3\sigma$ range (± 57 MeV/c^2) around the Λ_b^0 mass. The $\Lambda_c(2595)^+$ and $\Lambda_c(2625)^+$ signals are clearly visible. Although there are two possible Λ_c^{*+} candidates for each $\Lambda_b^0 \to \Lambda_c^+ \pi^- \pi^+ \pi^-$ decay, only the candidate made with the π^- with lower p_T has a value of $m(\Lambda_c^{*+}) - m(\Lambda_c^+)$ in the mass region where the $\Lambda_c(2595)^+$ and $\Lambda_c(2625)^+$ signals are expected. To check that the Λ_c^{*+} signal is entirely due to the $\Lambda_b^0 \to \Lambda_c^+ \pi^- \pi^+ \pi^-$ decay, we verified that the $m(\Lambda_c^{*+}) - m(\Lambda_c^+)$ distribution [Fig. 2(a), (yellow) filled histogram] for the Λ_b^0 candidates from the high-mass sideband of the $m(\Lambda_b^0) - m(\Lambda_c^+)$ distribution [Fig. 1(a)] has negligible statistics in the Λ_c^{*+} signal mass window. The $\Lambda_c(2595)^+$ and $\Lambda_c(2625)^+$ signal yields are estimated with an unbinned extended maximum-likelihood fit. The $\Lambda_c(2595)^+$ and $\Lambda_c(2625)^+$ signals are modeled with two nonrelativistic Breit-Wigner functions convolved with the same Gaussian resolution function, since the mass difference between the two resonances is tiny. The background is modeled by a linear function. The $\Lambda_c(2595)^+$ natural width is mass dependent to take into account the threshold effects, as reported in Ref. [14]. The $\Lambda_c(2625)^+$ natural width and the width of the Gaussian resolution function are free parameters of the fit. Table I reports the estimated signal yields and significances, evaluated by means of the likelihood ratio test, $LR \equiv L/L_{\rm bck}$, where L and $L_{\rm bck}$ are the likelihood of the signal and no-signal hypotheses, respectively [16].

Figures 2(b) and 2(c) show the $m(\Lambda_b^0) - m(\Lambda_c^+)$ distribution restricted to candidates with $m(\Lambda_c^{*+}) - m(\Lambda_c^+) < 0.325$ GeV/c^2 and $0.325 < m(\Lambda_c^{*+}) - m(\Lambda_c^+) < 0.360$ GeV/c^2, respectively, i.e. compatible with the $\Lambda_c(2595)^+$ and $\Lambda_c(2625)^+$ expected signals. Each signal is modeled with a Gaussian function, with floating mean and width. The combinatorial background is modeled with an exponential function with floating slope and normalization, and the physics background, which is mainly due to semileptonic $\Lambda_b^0 \to \Lambda_c^+ \pi^- \pi^+ l^- \bar{\nu}_l$ decays, is derived from simulation and introduced in the fit with fixed shape and floating normalization. We verified that the $\Lambda_b^0 \to \Lambda_c(2595)^+ \pi^-$ and $\Lambda_b^0 \to \Lambda_c(2625)^+ \pi^-$ yields estimated by fitting the $m(\Lambda_b^0) - m(\Lambda_c^+)$ distribution are compatible (with lower statistical significance) with the yields extracted from the resonance mass distributions and reported in Table I.

To extract the $\Lambda_b^0 \to \Sigma_c(2455)^{++} \pi^- \pi^-$ and $\Lambda_b^0 \to \Sigma_c(2455)^0 \pi^+ \pi^-$ signals, the contributions due to the $\Lambda_b^0 \to \Lambda_c(2595)^+ \pi^-$ and $\Lambda_b^0 \to \Lambda_c(2625)^+ \pi^-$ decay modes are removed by applying the veto requirement $m(\Lambda_c^{*+}) - m(\Lambda_c^+) > 0.380$ GeV/c^2. In Figs. 3(a) and 3(b) the resulting $m(\Sigma_c(2455)^{++}) - m(\Lambda_c^+)$ and $m(\Sigma_c(2455)^0) - m(\Lambda_c^+)$ distributions are shown. Prominent $\Sigma_c(2455)^{++}$ and $\Sigma_c(2455)^0$ signals are visible. While there is only one $\Sigma_c(2455)^{++}$ candidate for each $\Lambda_b^0 \to \Lambda_c^+ \pi^- \pi^+ \pi^-$ decay, two $\Sigma_c(2455)^0$ candidates are possible. Also in this case, only the candidate made with the π^- with lower p_T is in the $\Sigma_c(2455)^0$ mass region. The potential background contribution due to $\Sigma_c^{++,0}$ candidates not produced in $\Lambda_b^0 \to \Lambda_c^+ \pi^- \pi^+ \pi^-$ decays is excluded since the $m(\Sigma_c(2455)^{++,0}) - m(\Lambda_c^+)$ distributions ([yellow] filled

TABLE I. Yields and significances of the $\Lambda_b^0 \to \Lambda_c^+ \pi^- \pi^+ \pi^-$ decay modes. The quoted uncertainty is statistical only.

Λ_b^0 decay mode	Yield	Significance (σ)
$\Lambda_c(2595)^+ \pi^- \to \Lambda_c^+ \pi^- \pi^+ \pi^-$	46.0 ± 8.2	6.2
$\Lambda_c(2625)^+ \pi^- \to \Lambda_c^+ \pi^- \pi^+ \pi^-$	135 ± 15	>8
$\Sigma_c(2455)^{++} \pi^- \pi^- \to \Lambda_c^+ \pi^- \pi^+ \pi^-$	110 ± 19	6.6
$\Sigma_c(2455)^0 \pi^+ \pi^- \to \Lambda_c^+ \pi^- \pi^+ \pi^-$	36 ± 11	3.4
$\Lambda_c^+ \pi^- \pi^+ \pi^-$ (other)	790 ± 100	>8

histograms in Figs. 3(a) and 3(b)] obtained from the Λ_b^0 candidates in the higher mass sideband [Fig. 1(a)] show no evidence of a $\Sigma_c^{++,0}$ signal. The $\Sigma_c(2455)^{++}$ and $\Sigma_c(2455)^0$ signals are modeled with nonrelativistic Breit-Wigner functions convolved with a Gaussian resolution function, with the addition of an empirical background [17,18]. The $\Sigma_c(2455)^{++}$ and $\Sigma_c(2455)^0$ natural widths are Gaussian constrained to the world average values [3], while the width of the Gaussian resolution function is determined to be 1 MeV/c^2 from larger statistics samples of $\Sigma_c(2455)^{++}$ and $\Sigma_c(2455)^0$ in the Λ_b^0 lower mass region and is fixed in the fit. The effect of this approximation is taken into account in the systematic uncertainties. The estimated $\Lambda_b^0 \to \Sigma_c(2455)^{++}\pi^-\pi^-$ and $\Lambda_b^0 \to \Sigma_c(2455)^0\pi^+\pi^-$ yields and significances are reported in Table I.

In Figs. 3(c) and 3(d) the $m(\Lambda_b^0) - m(\Lambda_c^+)$ distributions are shown restricted to candidates with $0.160 < m(\Sigma_c(2455)^{++,0}) - m(\Lambda_c^+) < 0.176$ GeV/c^2, where the $\Sigma_c(2455)^{++}$ and $\Sigma_c(2455)^0$ signals are contained. The Λ_b^0 signal is modeled with a Gaussian distribution, with floating mean and width, while the combinatorial background is an exponential function with floating slope and

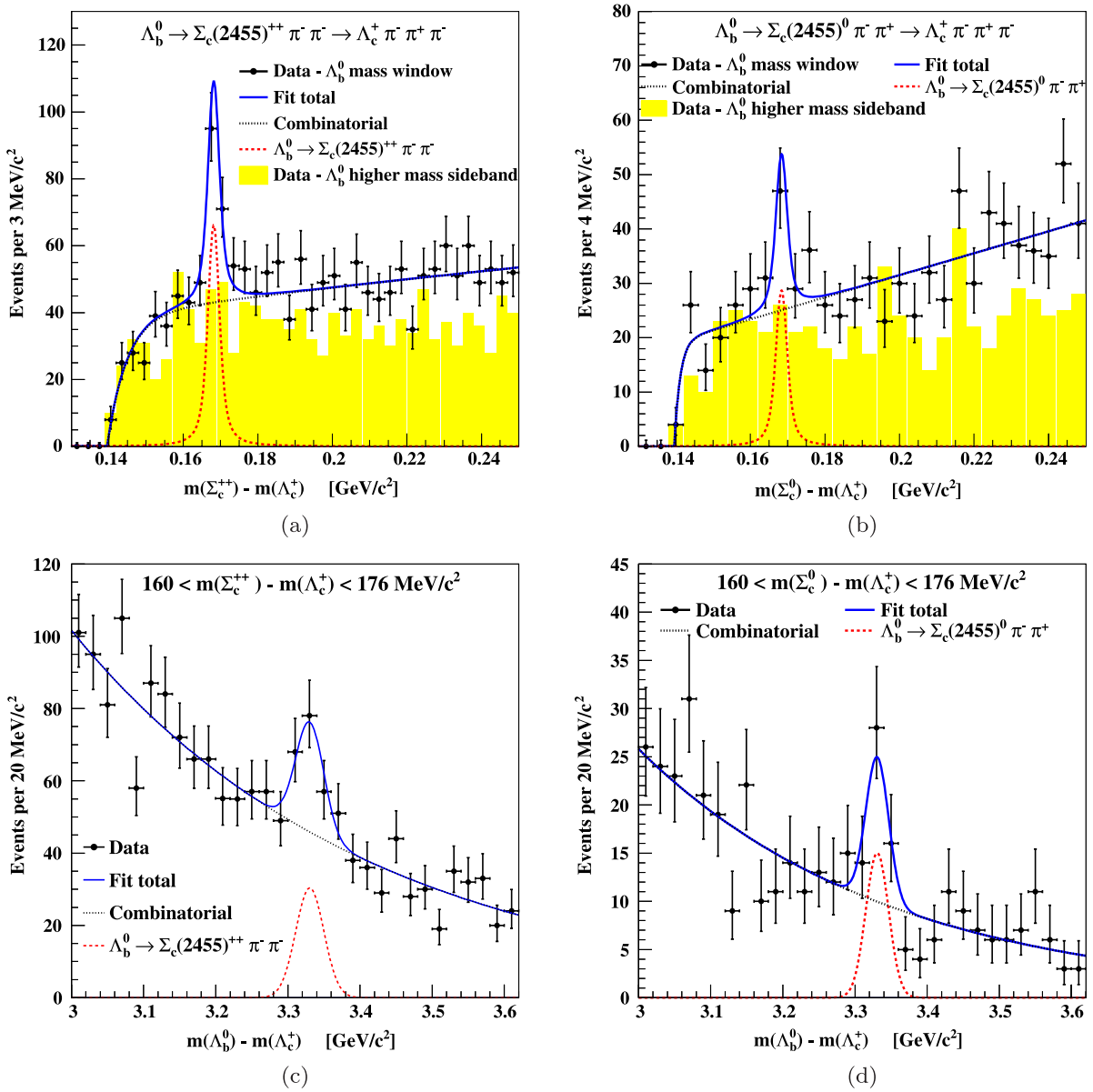

FIG. 3 (color online). The $\Lambda_b^0 \to \Sigma_c(2455)^{++}\pi^-\pi^-$ and $\Lambda_b^0 \to \Sigma_c(2455)^0\pi^+\pi^-$ signals: (a) $m(\Sigma_c(2455)^{++}) - m(\Lambda_c^+)$ distribution for candidates in a $\pm 3\sigma$ range ($\pm$ 57 MeV/c^2) around the Λ_b^0 mass; (b) $m(\Sigma_c(2455)^0) - m(\Lambda_c^+)$ distribution for candidates in a $\pm 3\sigma$ range around the Λ_b^0 mass; (c) $m(\Lambda_b^0) - m(\Lambda_c^+)$ distribution restricted to candidates in the region $0.160 < m(\Sigma_c(2455)^{++}) - m(\Lambda_c^+) < 0.176$ GeV/c^2; (d) $m(\Lambda_b^0) - m(\Lambda_c^+)$ distribution restricted to candidates in the region $0.160 < m(\Sigma_c(2455)^0) - m(\Lambda_c^+) < 0.176$ GeV/c^2.

normalization. We verified that the $\Lambda_b^0 \to \Sigma_c(2455)^{++}\pi^-\pi^-$ and $\Lambda_b^0 \to \Sigma_c(2455)^0\pi^+\pi^-$ yields estimated by fitting the $m(\Lambda_b^0) - m(\Lambda_c^+)$ distribution are compatible (with lower statistical significance) with the yields extracted from the resonance mass distributions and reported in Table I. The fitted masses and widths of the four resonances are in agreement with the world averages [3] and the recent CDF II measurements [14].

The residual Λ_b^0 signal (named $\Lambda_b^0 \to \Lambda_c^+\pi^-\pi^+\pi^-$(other)) is selected by applying the cuts $m(\Lambda_c^{*+}) - m(\Lambda_c^+) > 0.380\,\mathrm{GeV}/c^2$ and $m(\Sigma_c(2455)^{++,0}) - m(\Lambda_c^+) > 0.190\,\mathrm{GeV}/c^2$ to remove the contribution due to the resonant decay modes (Fig. 4). Monte Carlo simulation shows that the veto requirements reject 99% of the Λ_c^{*+} and $\Sigma_c(2455)^{++,0}$ yields, while retaining ~99% of the $\Lambda_b^0 \to \Lambda_c^+\pi^-\pi^+\pi^-$(other) signal. This residual Λ_b^0 signal is likely due to a combination of the $\Lambda_b^0 \to \Lambda_c^+ a_1(1260)^-$, $\Lambda_b^0 \to \Lambda_c^+\rho^0\pi^-$ with nonresonant $\rho^0\pi^-$ (i.e. not produced by an $a_1(1260)^-$ decay), and nonresonant $\Lambda_b^0 \to \Lambda_c^+\pi^-\pi^+\pi^-$ decay modes, in unknown proportions. A fit is performed with a Gaussian function, with floating mean and width to model the signal, an exponential function with floating slope and normalization to model the combinatorial background, and a physics background due to the $B_{(s)}^0 \to D_{(s)}^{(*)-}\pi^+\pi^-\pi^+$ decay modes, derived from simulation and included in the fit with fixed shape and floating normalization. The resulting yield is 790 ± 100 candidates (Table I). The unknown composition of the $\Lambda_b^0 \to \Lambda_c^+\pi^-\pi^+\pi^-$(other) sample is taken into account as a source of systematic uncertainty.

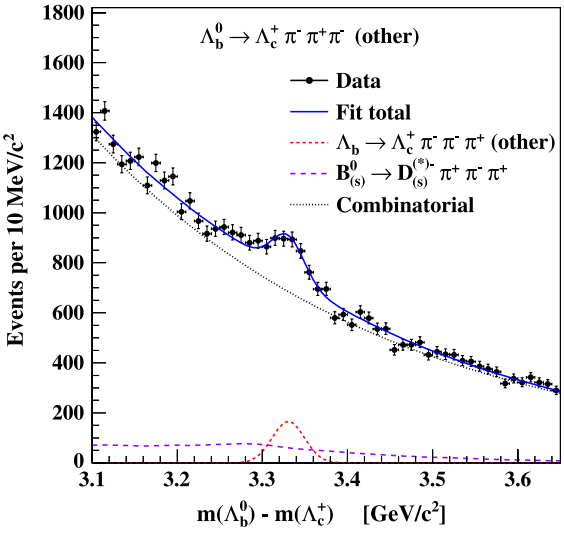

FIG. 4 (color online). The $\Lambda_b^0 \to \Lambda_c^+\pi^-\pi^+\pi^-$(other) signal after vetoing the resonant decay modes: $m(\Lambda_b^0) - m(\Lambda_c^+)$ distribution.

V. MEASUREMENT OF THE RATIO OF BRANCHING FRACTIONS $\mathcal{B}(\Lambda_b^0 \to \Lambda_c^+\pi^-\pi^+\pi^-)/\mathcal{B}(\Lambda_b^0 \to \Lambda_c^+\pi^-)$

We measure the following ratio of branching fractions:

$$\frac{\mathcal{B}(\Lambda_b^0 \to \Lambda_c^+\pi^-\pi^+\pi^-)}{\mathcal{B}(\Lambda_b^0 \to \Lambda_c^+\pi^-)} = \sum_i \frac{N(\Lambda_b^0 \to i \to \Lambda_c^+\pi^-\pi^+\pi^-)}{N(\Lambda_b^0 \to \Lambda_c^+\pi^-)} \times \frac{\epsilon_{\Lambda_b^0 \to \Lambda_c^+\pi^-}}{\epsilon_i}, \quad (1)$$

where N are the measured signal yields reported in Table I, and the sum on the intermediate "i" states includes $\Lambda_c(2595)^+\pi^-$, $\Lambda_c(2625)^+\pi^-$, $\Sigma_c(2455)^{++}\pi^-\pi^-$, $\Sigma_c(2455)^0\pi^+\pi^-$, and $\Lambda_c^+\pi^-\pi^+\pi^-$(other). In the last state, we assume equal proportions of the three decay modes $\Lambda_b^0 \to \Lambda_c^+ a_1(1260)^-$, $\Lambda_b^0 \to \Lambda_c^+\rho^0\pi^-$, and nonresonant $\Lambda_b^0 \to \Lambda_c^+\pi^-\pi^+\pi^-$. To convert event yields into relative branching fractions, we apply the corrections $\epsilon_{\Lambda_b^0 \to \Lambda_c^+\pi^-}/\epsilon_i$ for the various trigger and offline selection efficiencies of the decay modes $\Lambda_b^0 \to \Lambda_c^+\pi^-$ and $\Lambda_b^0 \to i \to \Lambda_c^+\pi^-\pi^+\pi^-$. All corrections are determined from the detailed detector simulation. The BGENERATOR program produces samples of specific B hadron decays according to measured p_T and rapidity spectra [19]. Decays of b and c hadrons and their daughters are simulated using the EVTGEN package [20]. The geometry and response of the detector components are simulated with the GEANT software package [21] and simulated events are processed with a full simulation of the CDF II detector and trigger. The $\Lambda_b^0 \to \Lambda_c^+\pi^-\pi^+\pi^-$ decay modes show different kinematics, due to the presence of two low-transverse-momentum pions in the $\Lambda_c^{*+} \to \Lambda_c^+\pi^-\pi^+$ decay, one low-transverse-momentum pion in the $\Sigma_c(2455)^{++,0} \to \Lambda_c^+\pi^{+,-}$ decay, and looser constraints in the $\Lambda_c^+\pi^-\pi^+\pi^-$(other) decays. These kinematic differences result in different corrections $\epsilon_{\Lambda_b^0 \to \Lambda_c^+\pi^-}/\epsilon_i$, 4.70 ± 0.10, 4.66 ± 0.10, 5.28 ± 0.11, and 18.49 ± 0.66, respectively, for the $\Lambda_c(2595)^+\pi^-$, $\Lambda_c(2625)^+\pi^-$, $\Sigma_c(2455)^{++}\pi^-\pi^-$, and $\Sigma_c(2455)^0\pi^+\pi^-$ decay modes, and 7.36 ± 0.18, 9.47 ± 0.25, and 11.64 ± 0.34, respectively, for the $\Lambda_b^0 \to \Lambda_c^+ a_1(1260)^-$, $\Lambda_b^0 \to \Lambda_c^+\rho^0\pi^-$, and nonresonant $\Lambda_b^0 \to \Lambda_c^+\pi^-\pi^+\pi^-$ decay modes. For the $\Lambda_c^+\pi^-\pi^+\pi^-$(other) decay mode, a correction factor equal to 9.16 ± 0.14 is obtained by combining the correction factors of the last three decay modes assumed in equal proportions.

With a similar method, we also measure the ratios of the branching fractions of the intermediate resonances contributing to $\Lambda_b^0 \to \Lambda_c^+\pi^-\pi^+\pi^-$:

$$\frac{\mathcal{B}(\Lambda_b^0 \to j \to \Lambda_c^+\pi^-\pi^+\pi^-)}{\mathcal{B}(\Lambda_b^0 \to \Lambda_c^+\pi^-\pi^+\pi^-)} = \frac{N(\Lambda_b^0 \to j \to \Lambda_c^+\pi^-\pi^+\pi^-)}{\sum_i N(\Lambda_b^0 \to i \to \Lambda_c^+\pi^-\pi^+\pi^-)\frac{\epsilon_j}{\epsilon_i}}. \quad (2)$$

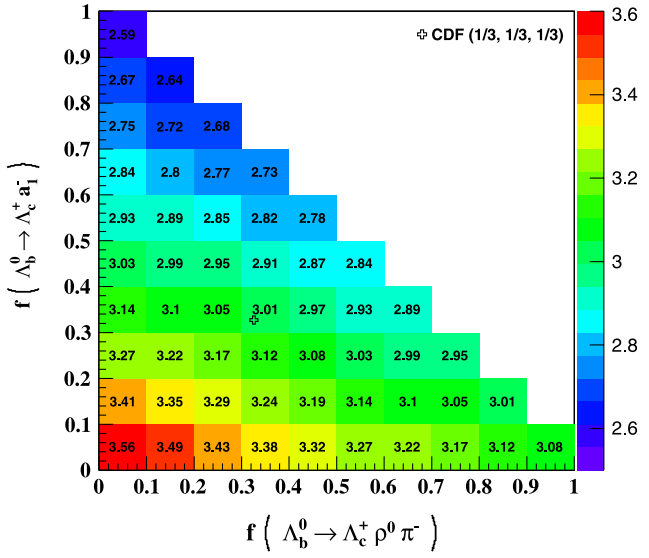

FIG. 5 (color online). $\mathcal{B}(\Lambda_b^0 \to \Lambda_c^+ \pi^- \pi^+ \pi^-)/\mathcal{B}(\Lambda_b^0 \to \Lambda_c^+ \pi^-)$ (gray [color] scale) as a function of the assumed fractions of $\Lambda_b^0 \to \Lambda_c^+ a_1^-$ and $\Lambda_b^0 \to \Lambda_c^+ \rho^0 \pi^-$ in the composition of the $\Lambda_b^0 \to \Lambda_c^+ \pi^- \pi^+ \pi^-$(other) sample. The central value of the ratio is overlaid in each bin. The fraction of nonresonant $\Lambda_b^0 \to \Lambda_c^+ \pi^- \pi^+ \pi^-$ is equal to $1 - f(\Lambda_b^0 \to \Lambda_c^+ a_1^-) - f(\Lambda_b^0 \to \Lambda_c^+ \rho^0 \pi^-)$. The cross represents the composition chosen for the present measurement assuming equal proportions of $\Lambda_b^0 \to \Lambda_c^+ a_1^-$, $\Lambda_b^0 \to \Lambda_c^+ \rho^0 \pi^-$ and nonresonant $\Lambda_b^0 \to \Lambda_c^+ \pi^- \pi^+ \pi^-$.

VI. SYSTEMATIC UNCERTAINTIES

The dominant sources of systematic uncertainty are the unknown relative fractions of $\Lambda_b^0 \to \Lambda_c^+ a_1(1260)^-$, $\Lambda_b^0 \to \Lambda_c^+ \rho^0 \pi^-$, and nonresonant $\Lambda_b^0 \to \Lambda_c^+ \pi^- \pi^+ \pi^-$, which affect the $\Lambda_b^0 \to \Lambda_c^+ \pi^- \pi^+ \pi^-$(other) decay mode efficiency, and the unknown Λ_b^0 production and Λ_c^+ decay polarizations, which affect the estimate of all the ϵ_i and $\epsilon_{\Lambda_b^0 \to \Lambda_c^+ \pi^-}$ efficiencies. The correction $\epsilon_{\Lambda_b^0 \to \Lambda_c^+ \pi^-}/\epsilon_{\Lambda_b^0 \to \Lambda_c^+ \pi^- \pi^+ \pi^-(\text{other})}$ has an average value of 9.16 and varies between a minimum of 7.36 and a maximum of 11.64, obtained in the extreme cases in which the $\Lambda_b^0 \to \Lambda_c^+ \pi^- \pi^+ \pi^-$(other) sample is assumed to be entirely composed of $\Lambda_b^0 \to \Lambda_c^+ a_1(1260)^-$ or nonresonant $\Lambda_b^0 \to \Lambda_c^+ \pi^- \pi^+ \pi^-$, respectively. The dependence of $\mathcal{B}(\Lambda_b^0 \to \Lambda_c^+ \pi^- \pi^+ \pi^-)/\mathcal{B}(\Lambda_b^0 \to \Lambda_c^+ \pi^-)$ on the fraction of $\Lambda_b^0 \to \Lambda_c^+ a_1(1260)^-$ and $\Lambda_b^0 \to \Lambda_c^+ \rho^0 \pi^-$ in the $\Lambda_b^0 \to \Lambda_c^+ \pi^- \pi^+ \pi^-$(other) sample is shown in Fig. 5. The difference between the values computed with the average and the minimum (maximum) efficiency correction, respectively, is taken as an estimate of the lower (upper) associated systematic uncertainty.

The unpolarized Λ_b^0 and Λ_c^+ simulation samples are used to obtain the central values of the efficiency corrections. For the study of the systematic uncertainties, angular distributions in simulation are reweighted according to all possible combinations of the Λ_b^0 production polarization states along the normal to the production plane with the Λ_c^+ polarization states. The Λ_b^0 polarization and the Λ_c^+ polarization are both taken to vary independently in the range ± 1. We assume the extreme scenarios where both the Λ_b^0 and Λ_c^+ baryons are 100% polarized and we recompute the efficiency corrections assuming the four possible Λ_b^0 and Λ_c^+ polarization combinations. The difference in the efficiency corrections between the simulation with reweighted angular distributions and the simulation with unpolarized Λ_b^0 and Λ_c^+ is used to determine the associated systematic uncertainty. These two sources of systematic uncertainty account for approximately 98% of the total systematic uncertainty on the measurement of the relative branching fraction $\mathcal{B}(\Lambda_b^0 \to \Lambda_c^+ \pi^- \pi^+ \pi^-)/\mathcal{B}(\Lambda_b^0 \to \Lambda_c^+ \pi^-)$. Other systematic errors stem from the uncertainties on the $\Lambda_b^0 \to \Lambda_c^+ \pi^-$ background shapes; on the Cabibbo suppressed decay mode contributions, which affect the estimate of the signal yields; and on the Monte Carlo simulation of the signal decay modes (limited sample statistics, trigger emulation, and Λ_b^0 production transverse momentum distribution), which affects the estimate of the efficiency corrections. The contributions due to the uncertainties on the Σ_c^{++} and Σ_c^0 signal and background shapes, the Λ_c^+ and Λ_c^{*+} branching fractions, and the Λ_b^0 and Λ_c^+ lifetimes are negligible.

As a cross-check of the analysis, we also measure the relative branching fraction $\mathcal{B}(B^0 \to D^- \pi^+ \pi^- \pi^+)/\mathcal{B}(B^0 \to D^- \pi^+)$, using the same data sample and vertex reconstruction procedure developed for the Λ_b^0 analysis. We apply the same optimized cuts to the B^0 candidates, with the additional request to have a D^- candidate with mass within $\pm 22\ \text{MeV}/c^2$ of the known mass of D^- [3]. We estimate $B^0 \to D^- \pi^+ \pi^- \pi^+$ and $B^0 \to D^- \pi^+$ yields of 431 ± 32 and 1352 ± 44 candidates, respectively. Our measurement $\mathcal{B}(B^0 \to D^- \pi^+ \pi^- \pi^+)/\mathcal{B}(B^0 \to D^- \pi^+) = 3.06 \pm 0.25(\text{stat})$ is in good agreement with the value calculated from the measured absolute branching fractions of the B^0 decay modes reported in Ref. [3].

VII. RESULTS

We measure the relative branching ratio of $\Lambda_b^0 \to \Lambda_c^+ \pi^- \pi^+ \pi^-$ to $\Lambda_b^0 \to \Lambda_c^+ \pi^-$ decays to be

$$\frac{\mathcal{B}(\Lambda_b^0 \to \Lambda_c^+ \pi^- \pi^+ \pi^-)}{\mathcal{B}(\Lambda_b^0 \to \Lambda_c^+ \pi^-)} = 3.04 \pm 0.33(\text{stat})^{+0.70}_{-0.55}(\text{syst}).$$

The relative branching fractions of the intermediate states contributing to $\Lambda_b^0 \to \Lambda_c^+ \pi^- \pi^+ \pi^-$ with respect to $\Lambda_b^0 \to \Lambda_c^+ \pi^-$ are reported in Table II. The absolute branching fractions are derived by normalizing to the known value $\mathcal{B}(\Lambda_b^0 \to \Lambda_c^+ \pi^-) = (8.8 \pm 3.2) \times 10^{-3}$ [22].

To compare our result with the recent LHCb measurement [5] of $1.43 \pm 0.16(\text{stat}) \pm 0.13(\text{syst})$, we assume the composition of the admixture to be two-thirds $\Lambda_b^0 \to$

TABLE II. Measured branching fractions relative to the $\Lambda_b^0 \to \Lambda_c^+ \pi^-$ decay mode (second column). Absolute branching fractions (third column) are derived by normalizing to the known value $\mathcal{B}(\Lambda_b^0 \to \Lambda_c^+ \pi^-) = (8.8 \pm 3.2) \times 10^{-3}$ [22]. The first quoted uncertainty is statistical, the second is systematic, and the third is due to the uncertainty on the $\Lambda_b^0 \to \Lambda_c^+ \pi^-$ branching fraction.

Λ_b^0 decay mode	Relative $\mathcal{B}$ to $\Lambda_b^0 \to \Lambda_c^+ \pi^-$	Absolute $\mathcal{B}(10^{-3})$
$\mathcal{B}(\Lambda_b^0 \to \Lambda_c(2595)^+ \pi^-) \cdot \mathcal{B}(\Lambda_c(2595)^+ \to \Lambda_c^+ \pi^+ \pi^-)$	$(7.1 \pm 1.3 \pm 0.6) \times 10^{-2}$	$0.62 \pm 0.11 \pm 0.05 \pm 0.23$
$\mathcal{B}(\Lambda_b^0 \to \Lambda_c(2625)^+ \pi^-) \cdot \mathcal{B}(\Lambda_c(2625)^+ \to \Lambda_c^+ \pi^+ \pi^-)$	$(20.6 \pm 2.4^{+1.4}_{-1.5}) \times 10^{-2}$	$1.81 \pm 0.21^{+0.12}_{-0.13} \pm 0.66$
$\mathcal{B}(\Lambda_b^0 \to \Sigma_c(2455)^{++} \pi^- \pi^-) \cdot \mathcal{B}(\Sigma_c(2455)^{++} \to \Lambda_c^+ \pi^+)$	$(19.0 \pm 3.3 \pm 1.1) \times 10^{-2}$	$1.67 \pm 0.29 \pm 0.10 \pm 0.61$
$\mathcal{B}(\Lambda_b^0 \to \Sigma_c(2455)^0 \pi^+ \pi^-) \cdot \mathcal{B}(\Sigma_c(2455)^0 \to \Lambda_c^+ \pi^-)$	$(21.5 \pm 6.5^{+4.5}_{-2.9}) \times 10^{-2}$	$1.89 \pm 0.57^{+0.40}_{-0.26} \pm 0.69$
$\mathcal{B}(\Lambda_b^0 \to \Lambda_c^+ \pi^- \pi^+ \pi^-(\text{other}))$	$2.36 \pm 0.32^{+0.68}_{-0.53}$	$20.8 \pm 2.8^{+6.0}_{-4.7} \pm 7.6$
$\mathcal{B}(\Lambda_b^0 \to \Lambda_c^+ \pi^- \pi^+ \pi^-)$	$3.04 \pm 0.33^{+0.70}_{-0.55}$	$26.8 \pm 2.9^{+6.2}_{-4.8} \pm 9.7$

TABLE III. Measured branching fractions of the resonant decay modes relative to $\Lambda_b^0 \to \Lambda_c^+ \pi^- \pi^+ \pi^-$. The first quoted uncertainty is statistical, the second is systematic.

Λ_b^0 decay mode	Relative $\mathcal{B}(10^{-2})$
$\mathcal{B}(\Lambda_b^0 \to \Lambda_c(2595)^+ \pi^-) \cdot \mathcal{B}(\Lambda_c(2595)^+ \to \Lambda_c^+ \pi^+ \pi^-)$	$2.3 \pm 0.5 \pm 0.4$
$\mathcal{B}(\Lambda_b^0 \to \Lambda_c(2625)^+ \pi^-) \cdot \mathcal{B}(\Lambda_c(2625)^+ \to \Lambda_c^+ \pi^+ \pi^-)$	$6.8 \pm 1.0 \pm 1.3$
$\mathcal{B}(\Lambda_b^0 \to \Sigma_c(2455)^{++} \pi^- \pi^-) \cdot \mathcal{B}(\Sigma_c(2455)^{++} \to \Lambda_c^+ \pi^+)$	$6.2 \pm 1.2 \pm 1.3$
$\mathcal{B}(\Lambda_b^0 \to \Sigma_c(2455)^0 \pi^+ \pi^-) \cdot \mathcal{B}(\Sigma_c(2455)^0 \to \Lambda_c^+ \pi^-)$	$7.1 \pm 2.1^{+1.5}_{-1.3}$
$\mathcal{B}(\Lambda_b^0 \to \Lambda_c^+ \pi^- \pi^+ \pi^-(\text{other}))$	$77.6 \pm 3.0^{+4.0}_{-4.1}$

$\Lambda_c^+ a_1(1260)^-$ and one-third $\Lambda_b^0 \to \Lambda_c^+ \rho^0 \pi^-$, and use the overall $\Lambda_b^0 \to \Lambda_c^+ \pi^- \pi^+ \pi^-$ yield and a global efficiency correction to compute $\mathcal{B}(\Lambda_b^0 \to \Lambda_c^+ \pi^- \pi^+ \pi^-)/\mathcal{B}(\Lambda_b^0 \to \Lambda_c^+ \pi^-)$, as in the LHCb analysis. This results in a value of $2.55 \pm 0.25(\text{stat})^{+0.82}_{-0.27}(\text{syst})$, which is inconsistent with the LHCb result at the level of 2.6 Gaussian standard deviations.

We also measure the relative branching fractions of the intermediate resonances contributing to the $\Lambda_b^0 \to \Lambda_c^+ \pi^- \pi^+ \pi^-$ decay (Table III). These results are of comparable or higher precision than existing measurements.

VIII. CONCLUSION

In summary, we reconstruct the $\Lambda_b^0 \to \Lambda_c^+ \pi^- \pi^+ \pi^-$ decay mode and the $\Lambda_b^0 \to \Lambda_c(2595)^+ \pi^-$, $\Lambda_b^0 \to \Lambda_c(2625)^+ \pi^-$, $\Lambda_b^0 \to \Sigma_c(2455)^{++} \pi^- \pi^-$, and $\Lambda_b^0 \to \Sigma_c(2455)^0 \pi^+ \pi^-$ resonant decay modes in CDF II data corresponding to 2.4 fb^{-1} of integrated luminosity. We measure the branching fraction of the resonant decay modes relative to the $\Lambda_b^0 \to \Lambda_c^+ \pi^-$ branching fraction. We also measure $\mathcal{B}(\Lambda_b^0 \to \Lambda_c^+ \pi^- \pi^+ \pi^-)/\mathcal{B}(\Lambda_b^0 \to \Lambda_c^+ \pi^-) = 3.04 \pm 0.33(\text{stat})^{+0.70}_{-0.55}(\text{syst})$. Using the known value of $\mathcal{B}(\Lambda_b^0 \to \Lambda_c^+ \pi^-)$ [22], we find $\mathcal{B}(\Lambda_b^0 \to \Lambda_c^+ \pi^- \pi^+ \pi^-) = (26.8 \pm 2.9(\text{stat})^{+6.2}_{-4.8}(\text{syst}) \pm 9.7(\text{norm})) \times 10^{-3}$, where the third quoted uncertainty arises from the $\Lambda_b^0 \to \Lambda_c^+ \pi^-$ normalization uncertainty.

ACKNOWLEDGMENTS

We thank the Fermilab staff and the technical staffs of the participating institutions for their vital contributions. This work was supported by the U.S. Department of Energy and National Science Foundation; the Italian Istituto Nazionale di Fisica Nucleare; the Ministry of Education, Culture, Sports, Science and Technology of Japan; the Natural Sciences and Engineering Research Council of Canada; the National Science Council of the Republic of China; the Swiss National Science Foundation; the A. P. Sloan Foundation; the Bundesministerium für Bildung und Forschung, Germany; the Korean World Class University Program, the National Research Foundation of Korea; the Science and Technology Facilities Council and the Royal Society, UK; the Russian Foundation for Basic Research; the Ministerio de Ciencia e Innovación, and Programa Consolider-Ingenio 2010, Spain; the Slovak R&D Agency; the Academy of Finland; and the Australian Research Council (ARC).

[1] A. V. Manohar and M. B. Wise, *Heavy Quark Physics*, Cambridge Monographs on Particle Physics, Nuclear Physics and Cosmology, Vol. 10, 1 (2007), ISBN 0-521-64241-8; N. Isgur, D. Scora, B. Grinstein, and M. B. Wise, Phys. Rev. D **39**, 799 (1989).

[2] I. Dunietz, Z. Phys. C **56**, 129 (1992).

[3] K. Nakamura *et al.* (Particle Data Group), J. Phys. G **37**, 075021 (2010).

[4] A. K. Leibovich, Z. Ligeti, I. W. Stewart, and M. B. Wise, Phys. Lett. B **586**, 337 (2004); H. Y. Cheng, Phys. Rev. D **56**, 2799 (1997).

[5] R. Aaij *et al.* (LHCb Collaboration), Phys. Rev. D **84**, 092001 (2011).

[6] D. Acosta *et al.* (CDF Collaboration), Phys. Rev. D **71**, 032001 (2005).

[7] A. Sill *et al.*, Nucl. Instrum. Methods Phys. Res., Sect. A **447**, 1 (2000).

[8] T. Affolder *et al.*, Nucl. Instrum. Methods Phys. Res., Sect. A **526**, 249 (2004).

[9] The pseudorapidity is defined as $\eta = -\log\tan(\theta/2)$, where θ is the angle between the trajectory of the particle being considered and the undeflected beam direction.

[10] CDF II uses a cylindrical coordinate system in which ϕ is the azimuthal angle, r is the radius from the nominal beam line, and z points in the proton beam direction, with the origin at the center of the detector. The transverse plane is the plane perpendicular to the z axis.

[11] E. Thomson *et al.*, IEEE Trans. Nucl. Sci. **49**, 1063 (2002).

[12] B. Ashmanskas *et al.*, Nucl. Instrum. Methods Phys. Res., Sect. A **518**, 532 (2004); L. Ristori and G. Punzi, Annu. Rev. Nucl. Part. Sci. **60**, 595 (2010).

[13] Throughout this article, the inclusion of charge conjugate decays is implied.

[14] T. Aaltonen *et al.* (CDF Collaboration), Phys. Rev. D **84**, 012003 (2011).

[15] T. Aaltonen *et al.* (CDF Collaboration), Phys. Rev. Lett. **104**, 102002 (2010).

[16] R. Royall, J. Am. Stat. Assoc. **95**, 760 (2000).

[17] R. Brun and F. Rademakers, Nucl. Instrum. Methods Phys. Res., Sect. A **389**, 81 (1997). See also http://root.cern.ch/.

[18] I. Antcheva *et al.*, Comput. Phys. Commun. **180**, 2499 (2009).

[19] P. Nason, S. Dawson, and R. K. Ellis, Nucl. Phys. **B303**, 607 (1988); Nucl. Phys. **B327**, 49 (1989); C. Peterson, D. Schlatter, I. Schmitt, and P. M. Zerwas, Phys. Rev. D **27**, 105 (1983).

[20] D. J. Lange, Nucl. Instrum. Methods Phys. Res., Sect. A **462**, 152 (2001).

[21] R. Brun, R. Hagelberg, M. Hansroul, and J. C. Lassalle, CERN Report No. CERN-DD-78-2-REV, 1978 (unpublished).

[22] A. Abulencia *et al.* (CDF Collaboration), Phys. Rev. Lett. **98**, 122002 (2007).